Suppression of the bulk high spin–low spin transition by doping the chiral magnet MnGe

N. Martin, M. Deutsch, T. Hansen, M. T Fernandez-Diaz, L. Fomicheva, A. Tsvyashchenko, I. Mirebeau

Rapid Communications

Suppression of the bulk high spin–low spin transition by doping the chiral magnet MnGe

N. Martin,[1,*] M. Deutsch,[2] T. C. Hansen,[3] M. T. Fernandez-Diaz,[3] L. N. Fomicheva,[4] A. V. Tsvyashchenko,[4] and I. Mirebeau[1]

[1]*Laboratoire Léon Brillouin, CEA, CNRS, Université Paris-Saclay, CEA Saclay 91191 Gif-sur-Yvette, France*

[2]*Université de Lorraine, CNRS, CRM2, Nancy, France*

[3]*Institut Laue Langevin, BP156, F-38042 Grenoble, France*

[4]*Vereshchagin Institute for High Pressure Physics, Russian Academy of Sciences, 142190, Troitsk, Moscow, Russia*

(Received 14 May 2019; published 5 August 2019)

In the MnGe chiral magnet, the helimagnetic order and local moment collapse in two steps, showing the succession of high spin (HS) and low spin (LS) states as pressure increases. Here, we use high-pressure neutron diffraction to study the doped compounds $Mn_{0.86}Co_{0.14}Ge$ and $Mn_{0.9}Rh_{0.1}Ge$, and show that the evolution of their microscopic magnetic properties is instead continuous. It means that the bulk HS-LS transition is a unique feature of pure MnGe, very sensitive to small changes of the band structure and easily suppressed by chemical substitution. On the other hand, the helimagnetic correlations appear to be strengthened by doping and survive up to larger pressures (≈19 GPa, to be compared with ≈13 GPa). We discuss these results in the light of other disordered systems with remarkable properties, the so-called Invar alloys.

DOI: 10.1103/PhysRevB.100.060401

In itinerant magnets, the strong sensitivity of the magnetic moment to fine details of the band structure may result in magnetic states which become energetically equivalent for certain values of the lattice constant. This can, for instance, lead to electronic transitions, between a high spin (HS) state (with a large specific volume) toward a low spin (LS) state (with smaller volume), that can be observed by varying either temperature or pressure. One of the most spectacular consequences of such phenomenon is believed to be the Invar effect [1,2], discovered by Guillaume in Fe-Ni alloys [3], with numerous industrial applications. Other examples of HS-LS transitions can be found in molecular compounds containing transition metals atoms [4] (Co, Fe, Mn), such as the Prussian blues analogs [5], due to the strong sensitivity of the crystal field to external parameters (pressure, temperature, or light).

Helical magnets with a noncentrosymmetric space group, such as MnSi or FeGe, are textbook examples of itinerant magnetism, hosting skyrmion lattices and being highly sensitive to pressure and chemical substitution. Their helimagnetic ground states are built upon a hierarchical energy scheme involving ferromagnetic (FM) exchange, Dzyaloshinskii-Moriya (DM) interaction, and crystalline anisotropy energies [6]. It collapses under pressure, yielding non-Fermi liquid behavior and partial ordering of fluctuating magnetic moments [7,8].

In this family, MnGe stands as an exception. Its short helical period of ≈30 Å [9,10] cannot be explained by a bare competition between a FM exchange and DM interactions, since it would require an unphysically large spin-orbit coupling. Recent experiments suggest the presence of a *3d* soliton lattice without need of a magnetic field [11], possibly triggered by topological chiral interactions [12]. Strikingly, when applying pressure, the magnetic order and local moment of MnGe collapse in two steps, through HS and LS states [13], followed by a zero spin (ZS) state [14]. This peculiar behavior was predicted by *ab initio* calculations [15], showing rigid shifts of the spin-split bands upon compression. The HS-LS transition is associated with irreversibilities of the lattice constant [14], strongly recalling Invar anomalies [16,17].

Under chemical substitution of Mn for *3d*-Co or *4d*-Rh atoms, helical order in MnGe strongly changes, showing the onset of very long period structures above a certain doping level ($x > 0.3$ and 0.5 for Rh and Co, respectively), with characteristics similar to certain cholesteric liquid crystals [18]. These substitutions yield either a compression (Co) or a dilatation (Rh) of the cubic lattice constant a. At lower doping, when MnGe helical order is preserved, one could then expect that the chemical pressure resulting from the substitution would either enhance (Co) or counteract (Rh) the effect of the applied pressure. This should yield a shift of the HS-LS transition (situated at $p_{C1} \approx 6$ GPa in pure MnGe) toward lower (Co) or higher (Rh) pressures, depending on the nature of the substituting ion.

In order to check the above scenario, we have used high-pressure neutron diffraction to study two samples with low doping level, namely, $Mn_{0.86}Co_{0.14}Ge$ and $Mn_{0.9}Rh_{0.1}Ge$. From the lattice constants at ambient pressure and at $T = 1.5$ K ($a = 4.767$ Å for $Mn_{0.86}Co_{0.14}Ge$ and 4.794 Å for $Mn_{0.9}Rh_{0.1}Ge$ [18]), one should expect pressure shifts of −1.8 GPa for Co doping and +0.9 GPa for Rh doping with respect to MnGe ($a = 4.785$ Å). Strikingly, instead of a rigid shift of the critical pressure, we observe a *complete smearing* of the transitions in both cases. The helical period and ground state magnetic moment gradually decrease without showing any critical behavior in the studied pressure range (i.e., up to 9 GPa). Moreover, the magnetic moments of the two compounds vary in very similar ways and do not universally

*nicolas.martin@cea.fr

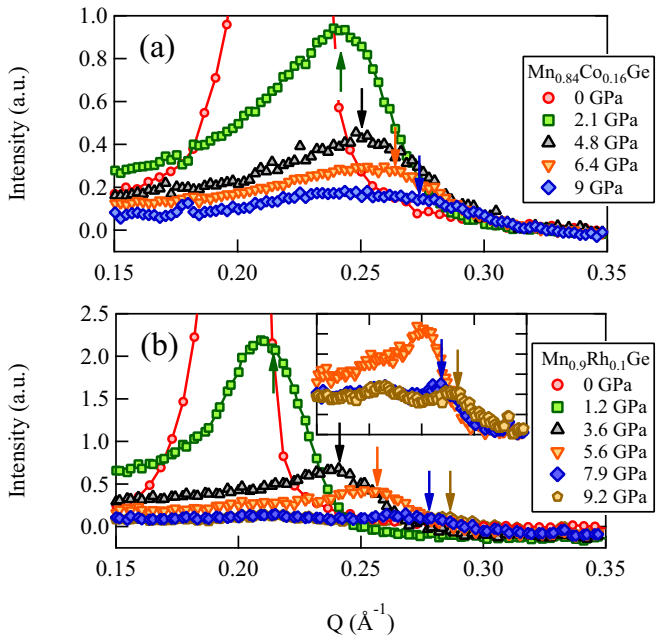

FIG. 1. Small-angle part of the NPD patterns of $Mn_{0.86}Co_{0.14}Ge$ (a) and $Mn_{0.9}Rh_{0.1}Ge$ (b), measured with a neutron wavelength $\lambda = 2.41$ Å at low temperature ($T < 10$ K) and for different applied pressures. The patterns are here corrected from a constant background and scaled to the intensity of the nuclear (110) peak in order to ease comparison. The strong helimagnetic peak asymmetry arises from the horizontal incoming beam divergence. Arrows show its position, as deduced from the Rietveld refinements [19]. The inset of (b) shows the magnetic signals recorded at the highest pressures in $Mn_{0.9}Rh_{0.1}Ge$. The Q range is the same as in the main panels.

scale with the unit cell volume. These results show that the HS-LS transition is very fragile and easily destroyed by chemical disorder, yielding a progressive breakdown of the Mn magnetism under pressure.

We have studied powder samples, synthesized under high pressure and high temperature [20], on the high-intensity diffractometer D20 of the Institut Laue Langevin [21]. The samples were inserted in a Paris-Edimburgh press, using a (4:1) deuterated methanol-ethanol mixture as transmitting pressure medium. A Pb chip was inserted in the cell to calibrate the applied pressure *in situ*, by monitoring the evolution of the Pb lattice constant [22]. The temperature was varied between ≈6 and 300 K. Pressure changes were systematically performed above the solid-liquid transition of the transmitting medium, to ensure quasihydrostatic pressure. Neutron powder diffraction (NPD) patterns, corrected from background and detector efficiency, were refined using the FULLPROF suite [23].

Patterns focusing on the main helical peak (i.e., the satellite of the $Q = 0$ Bragg peak), measured at the lowest temperatures ($T < 10$ K) are shown in Fig. 1. To be easily compared, data obtained at different pressures are corrected from a constant background then scaled to the integrated intensity of the nuclear Bragg peak (110). Figure 1 shows that in both samples, the intensity of the $Q = 0$ satellite strongly decreases under pressure, whereas its positions moves toward high angles. This gradual evolution takes place up to the highest measured pressure, without saturation of the peak intensity or blocking of the peak position. It shows that both magnetic moment and helical wavelength, respectively related to the peak intensity and peak position, continuously vary in the studied pressure range. This behavior strongly contrasts with observations in pure MnGe, where the peak intensity and position become independent of the applied pressure above $p_{C1} \approx 6$ GPa, marking the HS-LS transition (see Fig. 3 of Ref. [13]). Thus, data displayed in Fig. 1 are already a clear indication of the smearing of this transition in the substituted samples.

For each pressure, a series of patterns was measured versus temperature. Typical examples are shown in the Supplemental Material [19], together with joint Rietveld refinements of the crystal and magnetic structures. The $Q = 0$ satellite coexists with the Bragg peaks from the crystal structure at higher Q values. As in MnGe, satellites of the other Bragg reflections are much less intense and cannot be detected under pressure, since the signal-to-noise ratio is degraded by the background contribution from the pressure cell and small sample volume. Good refinements are obtained by assuming that the same type of helical order persists in the whole studied temperature and pressure (0–9 GPa) range. Taking the calculated resolution of the spectrometer into account, the helical peaks shows a small broadening with respect to the nuclear peaks, which increases with increasing pressure. From this broadening, one can extract the helimagnetic correlation lengths. They always remain much larger than the helical periodicities, suggesting well-preserved medium-to-long range magnetic ordering up to the highest pressure in both samples [19].

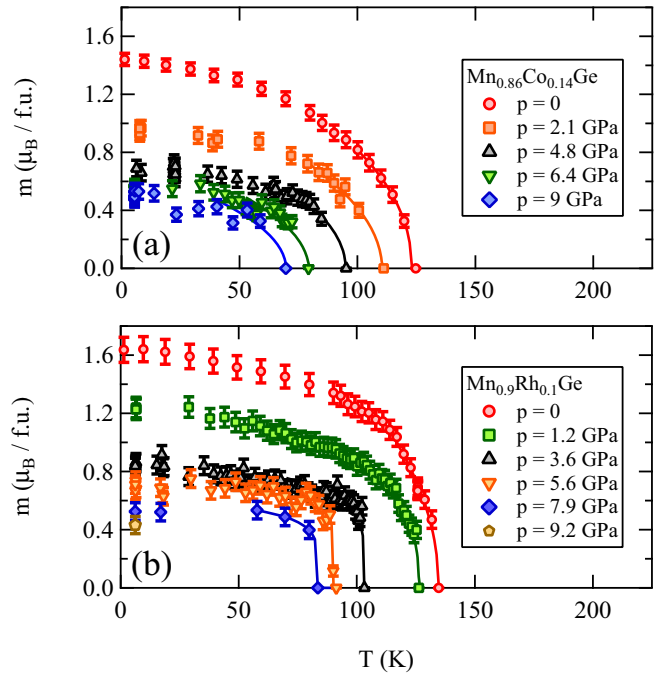

FIG. 2. Temperature dependence of the ordered magnetic moments per formula unit (f.u.) in $Mn_{0.86}Co_{0.14}Ge$ (a) and $Mn_{0.9}Rh_{0.1}Ge$ (b) for different applied pressures. The solid lines are fits of Eq. (1) to the data, performed in a temperature range limited to the vicinity of T_N (see text).

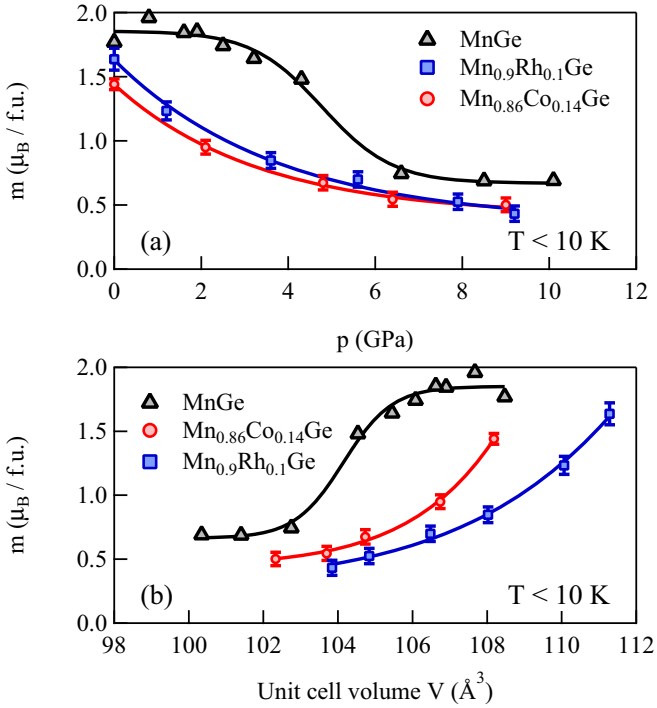

FIG. 3. Ordered magnetic moment per formula unit (f.u.) in $Mn_{0.86}Co_{0.14}Ge$, $Mn_{0.9}Rh_{0.1}Ge$, and MnGe, as a function of pressure p (a) and unit cell volume V in (b). Data for pure MnGe are taken from Ref. [13].

Thanks to the refinements, the intensity of the helical peak can be properly scaled to the intensity of the nuclear peaks, yielding a determination of the ordered moment m in absolute units. Its temperature dependence is plotted for each measured pressure in Fig. 2. In the vicinity of the ordering (Néel) temperature T_N, data are tentatively described by a power law

$$m(T) = \begin{cases} a & (1 - T/T_N)^{\beta} \quad \text{for } T \leqslant T_N \\ 0 & \text{otherwise,} \end{cases} \tag{1}$$

where a is a scaling factor and β a critical exponent. m decreases continuously with increasing temperature in both cases. Its variation is rather smooth in the Co sample ($\beta = 0.5$ as in pure MnGe), whereas it is much more abrupt in the Rh sample ($\beta \approx 0.2$), recalling a first-order transition.

The pressure dependence of the ordered magnetic moment at the lowest temperature ($T < 10$ K $\ll T_N$) is shown in Fig. 3(a) for the two samples, in comparison with previous results in pure MnGe [24]. At ambient pressure, the magnetic moments are slightly decreased in the doped samples, as expected from magnetic dilution. But as a main result, we find that their pressure dependence strongly differs from that of MnGe. In MnGe, the moment retains its HS value of $\approx 1.9\mu_B$ from ambient pressure up to $p_{C1} \approx 6$ GPa, then shows a steplike decrease toward its LS value of $\approx 0.6\mu_B$, which remains constant up to the maximum pressure of 10.1 GPa. For the two substituted samples, the moment starts to decrease *from the lowest applied pressure* which amounts to 1.2 and 2.1 GPa for Co and Rh samples, respectively. In other words, the critical pressure p_{C1} which separates the HS from the LS state in MnGe vanishes under doping.

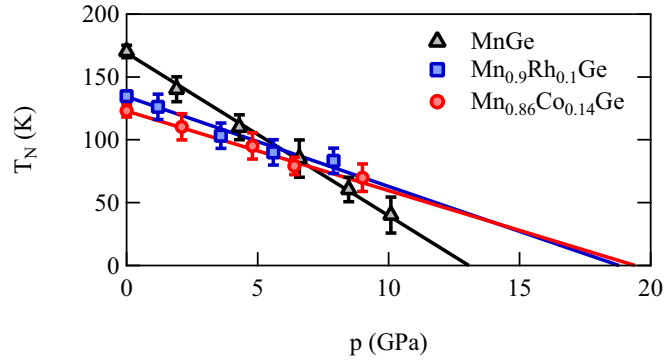

FIG. 4. Néel temperature T_N versus pressure as measured in $Mn_{0.86}Co_{0.14}Ge$ and $Mn_{0.9}Rh_{0.1}Ge$. The values of T_N in MnGe from Ref. [13] are plotted for comparison.

From the (p, V) equations of state, determined in MnGe from neutron and x-ray synchrotron data [13,25], and from neutrons in the doped samples [19], one can also plot the variation of the moment versus the unit cell volume [Fig. 3(b)]. As another important result, the pressure dependence of the moments are very similar in the Co and Rh samples with similar amount of doping, and they do not fall on a universal curve, scaling with the unit cell volumes. It means that the parameter which governs the suppression of the HS-LS transition is not the chemical pressure but most likely the magnetic disorder induced by Co and Rh ions which bear weak magnetic moments, either intrinsic [18] or induced [26]. We note that a rather smooth evolution of the saturated moment was recently reported in $MnSi_{1-x}Ge_x$, in relation to an ≈5% change of lattice constant [27]. There also, one should account for the effective magnetic contribution of Ge [26] and for the influence of disorder on the band structure to capture the nature of the observed transition.

For each pressure, fits of Eq. (1) to the temperature dependence of the magnetic moment (Fig. 2) in the hig-temperature range determine the Néel temperature T_N from the helical to the paramagnetic state where the ordered moment vanishes. In all samples, T_N decreases linearly with the applied pressure (Fig. 4) but the slope for MnGe (-12.9 ± 1.0 K GPa^{-1}) is about twice higher than for the doped samples, namely, -6.3 ± 1.0 K GPa^{-1} for Co and -7.2 ± 1.1 K GPa^{-1} for Rh. Extrapolation of these linear variations to $T_N = 0$ yields a quantum critical point (QCP) at p_0, where the ordered moment vanishes. In MnGe, $p_0 = 13.1(7)$ GPa is situated in the medium pressure range between two QCPs, namely, $p_{C1} \approx 6$ GPa which marks the HS-LS transition and $p_{C2} \approx 23$ GPa which corresponds to the Mn moment collapse [25]. On the contrary, in the doped samples where $p_{C1} \approx 0$, p_0 extrapolates toward very high values, of 19.4 ± 2.0 GPa for Co and 18.8 ± 1.6 GPa for Rh, in the pressure range of p_{C2}. This is another sign of the smearing of the HS-LS transition by doping.

We finally turn to the helical wavelength λ_h, deduced from the wave vector Q_h of the helical pitch ($\lambda_h = 2\pi/Q_h$). It exhibits a smooth dependence with pressure in the doped samples, and gradually decreases with unit cell volume without any anomaly (Fig. 5). This is not the case for MnGe [13], where λ_h saturates at a constant value of ≈20 Å above

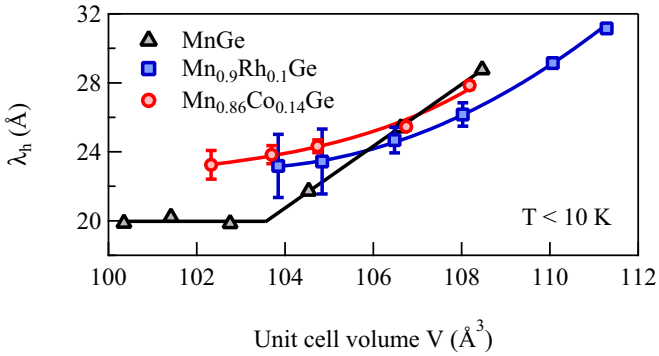

FIG. 5. Helical wavelength λ_h in $Mn_{0.86}Co_{0.14}Ge$, $Mn_{0.9}Rh_{0.1}Ge$, and MnGe versus the unit cell volume V. The values in MnGe are from Ref. [13].

6 GPa, or equivalently for a unit cell volume V_0 smaller than $\approx$104 Å^3, showing the occurrence of the LS state.

To understand the suppression of the bulk HS-LS transition by doping in MnGe, we propose the following scenario, based on analogy with random Invar alloys [28,29]. At ambient pressure, the substituted Co/Rh atoms with low magnetic moments locally breaks the short period helical structure in MnGe, issued from a competition of near-neighbor interactions [30]. At the same time they induce different magnetic environments for the Mn atoms, depending on the number of their Co/Rh near neighbors. The sensitivity of the magnetic moments and exchange interactions to these local environments results in a local spin canting of the Mn moments with respect to the average helical angle. Upon a small increase of pressure, the atomic volume decreases and LS moments become energetically favored at some peculiar sites, since the Co/Rh impurities act as nucleation centers to trigger the HS-LS transition locally. The HS state, stable at ambient pressure, starts to compete with a large number of magnetic configurations which are energetically equivalent, yielding magnetic frustration. These partly disordered configurations involve both local canting and LS moments. As pressure increases further, the distribution of canting angles increases together with the number of LS moments, so that the average ordered and local moments decrease at the same time. Consequently, the pressure p_0 where the helical order vanishes is close to the pressure p_{C2} which marks the disappearance of the local moment or ZS state. The evolution toward the ZS state is gradual and continuous, due to the large distribution of both canting angles and HS/LS spin states, correlated to the local chemical environments.

Recent *ab initio* calculations suggest to interpret the pressure-induced Invar effect in disordered Fe-Ni alloys in a similar way [31,32]. In this picture, a continuous transition occurs between a HS ferromagnetic state at high volume and an increasing number of noncollinear and partly disordered configurations at low volumes, nucleated by locally "flipped" moments. In Fe-Ni alloys, the ability of the system to relax its magnetic structure among these configurations could explain the suppression of anharmonic phonon modes and the low thermal expansion associated with the Invar effect. Similarly in MnGe the Co/Rh doping could affect not only the magnetic structure and the pressure-induced transition, but also the low-energy spin dynamics [11,24,25], the phonon spectrum, and the elastic properties. This could be checked in future experiments.

In conclusion, a moderate substitution of Mn for Co or Rh suppresses the pressure-induced HS-LS transition in the MnGe helical magnet, instead of shifting it toward lower (Co) or higher (Rh) pressures as expected from bare chemical pressure effects. This shows that the main effect of doping is the magnetic disorder induced by the low Co/Rh moments, randomly distributed in the Mn helical structure. Under pressure, the gradual evolution of the helical state toward paramagnetism suggests the occurrence of disordered configurations, involving local canting and reduced moments, recalling the behavior of disordered Invar alloys.

We thank P. Bonville for the magnetic measurements, as well as J. Maurice and C. Payre for provision of the high-pressure setup on the D20 diffractometer (ILL). A.V.T. is grateful to the Russian Science Foundation (Grant No. 17-12-01050).

[1] R. Weiss, Proc. Phys. Soc. **82**, 281 (1963).
[2] V. L. Moruzzi, Phys. Rev. B **41**, 6939 (1990).
[3] C. E. Guillaume, C. R. Hebd. Séances Acad. Sci. **125**, 235 (1897).
[4] L. Catala, F. Volatron, D. Brinzei, and T. Mallah, Inorg. Chem. **48**, 3360 (2009).
[5] A. Bleuzen, C. Lomenech, V. Escax, F. Villain, F. Varret, C. Cartier dit Moulin, and M. Verdaguer, J. Am. Chem. Soc. **122**, 6648 (2000).
[6] J. Kishine and A. Ovchinnikov, in *Solid State Physics*, edited by R. E. Camley and R. L. Stamps (Academic, New York, 2015), Vol. 66, pp. 1–130.
[7] C. Pfleiderer, D. Reznik, L. Pintschovius, H. v. Lohneysen, M. Garst, and A. Rosch, Nature (London) **427**, 227 (2004).
[8] A. Barla, H. Wilhelm, M. K. Forthaus, C. Strohm, R. Rüffer, M. Schmidt, K. Koepernik, U. K. Rößler, and M. M. Abd-Elmeguid, Phys. Rev. Lett. **114**, 016803 (2015).
[9] N. Kanazawa, Y. Onose, T. Arima, D. Okuyama, K. Ohoyama, S. Wakimoto, K. Kakurai, S. Ishiwata, and Y. Tokura, Phys. Rev. Lett. **106**, 156603 (2011).
[10] O. L. Makarova, A. V. Tsvyashchenko, G. André, F. Porcher, L. N. Fomicheva, N. Rey, and I. Mirebeau, Phys. Rev. B **85**, 205205 (2012).
[11] N. Martin, I. Mirebeau, C. Franz, G. Chaboussant, L. N. Fomicheva, and A. V. Tsvyashchenko, Phys. Rev. B **99**, 100402(R) (2019).
[12] S. Grytsiuk, J.-P. Hanke, M. Hoffmann, J. Bouaziz, O. Gomonay, G. Bihlmayer, S. Lounis, Y. Mokrousov, and S. Blügel, arXiv:1904.02369.

[13] M. Deutsch, O. L. Makarova, T. C. Hansen, M. T. Fernandez-Diaz, V. A. Sidorov, A. V. Tsvyashchenko, L. N. Fomicheva, F. Porcher, S. Petit, K. Koepernik *et al.*, Phys. Rev. B **89**, 180407(R) (2014).

[14] N. Martin, M. Deutsch, J.-P. Itié, J.-P. Rueff, U. K. Rössler, K. Koepernik, L. N. Fomicheva, A. V. Tsvyashchenko, and I. Mirebeau, Phys. Rev. B **93**, 214404 (2016).

[15] U. K. Rössler, J. Phys.: Conf. Ser. **391**, 012104 (2012).

[16] E. Wasserman, *Handbook of Ferromagnetic Materials* (Elsevier, New York, 1990), Vol. 5, pp. 237–322.

[17] P. Gorria, D. Martínez-Blanco, M. J. Pérez, J. A. Blanco, A. Hernando, M. A. Laguna-Marco, D. Haskel, N. Souza-Neto, R. I. Smith, W. G. Marshall *et al.*, Phys. Rev. B **80**, 064421 (2009).

[18] N. Martin, M. Deutsch, G. Chaboussant, F. Damay, P. Bonville, L. N. Fomicheva, A. V. Tsvyashchenko, U. K. Rössler, and I. Mirebeau, Phys. Rev. B **96**, 020413(R) (2017).

[19] See Supplemental Material at http://link.aps.org/supplemental/10.1103/PhysRevB.100.060401 for information concerning the samples studied in the Rapid Communication and additional details concerning the treatment of the high-pressure neutron diffraction data, which includes Refs. [33–37].

[20] A. Tsvyashchenko, V. Sidorov, L. Fomicheva, V. Krasnorussky, R. Sadykov, J. Thompson, K. Gofryk, F. Ronning, and V. Ivanov, in *Magnetism and Magnetic Materials V*, Solid State Phenomena (Scientific.Net, Zurich, Switzerland, 2012), Vol. 190, pp. 225–228.

[21] T. C. Hansen, P. F. Henry, H. E. Fischer, J. Torregrossa, and P. Convert, Meas. Sci. Technol. **19**, 034001 (2008).

[22] S. Klotz, *Techniques in High Pressure Neutron Scattering* (CRC, Boca Raton, FL, 2012).

[23] J. Rodrìguez-Carvajal, Physica B **192**, 55 (1993).

[24] M. Deutsch, P. Bonville, A. V. Tsvyashchenko, L. N. Fomicheva, F. Porcher, F. Damay, S. Petit, and I. Mirebeau, Phys. Rev. B **90**, 144401 (2014).

[25] N. Martin, M. Deutsch, F. Bert, D. Andreica, A. Amato, P. Bonfà, R. De Renzi, U. K. Rößler, P. Bonville, L. N. Fomicheva *et al.*, Phys. Rev. B **93**, 174405 (2016).

[26] V. A. Sidorov, A. E. Petrova, N. M. Chtchelkatchev, M. V. Magnitskaya, L. N. Fomicheva, D. A. Salamatin, A. V. Nikolaev, I. P. Zibrov, F. Wilhelm, A. Rogalev *et al.*, Phys. Rev. B **98**, 125121 (2018).

[27] Y. Fujishiro, N. Kanazawa, T. Nakajima, X. Z. Yu, K. Ohishi, Y. Kawamura, K. Kakurai, T. Arima, H. Mitamura, A. Miyake *et al.*, Nat. Commun. **10**, 1059 (2019).

[28] M. van Schilfgaarde, I. Abrikosov, and B. Johansson, Nature (London) **400**, 46 (1999).

[29] L. Dubrovinsky, N. Dubrovinskaia, I. A. Abrikosov, M. Vennström, F. Westman, S. Carlson, M. van Schilfgaarde, and B. Johansson, Phys. Rev. Lett. **86**, 4851 (2001).

[30] V. A. Chizhikov and V. E. Dmitrienko, Phys. Rev. B **88**, 214402 (2013).

[31] A. V. Ruban, M. I. Katsnelson, W. Olovsson, S. I. Simak, and I. A. Abrikosov, Phys. Rev. B **71**, 054402 (2005).

[32] I. A. Abrikosov, A. E. Kissavos, F. Liot, B. Alling, S. I. Simak, O. Peil, and A. V. Ruban, Phys. Rev. B **76**, 014434 (2007).

[33] A. Berche, J. Tedenac, and P. Jund, Intermetallics **47**, 23 (2014).

[34] M. Regulski, R. Przeniosło, I. Sosnowska, D. Hohlwein, and R. Schneider, J. Alloys Compd. **362**, 236 (2004).

[35] R. Viennois, C. Reibel, D. Ravot, R. Debord, and S. Pailhès, Europhys. Lett. **111**, 17008 (2015).

[36] S. Klotz, T. Strässle, G. Rousse, G. Hamel, and V. Pomjakushin, Appl. Phys. Lett. **86**, 031917 (2005).

[37] S. Klotz, L. Paumier, G. L. March, and P. Munsch, High Press. Res. **29**, 649 (2009).

Supplementary material for

"Suppression of the bulk high spin-low spin transition by doping the MnGe chiral magnet"

N. Martin,[1] M. Deutsch,[2] T.C. Hansen,[3] M.T. Fernandez-Diaz,[3]

L. N. Fomicheva,[4] A. V. Tsvyashchenko,[4] and I. Mirebeau[1]

[1]*Laboratoire Léon Brillouin, CEA, CNRS, Université Paris-Saclay, CEA Saclay 91191 Gif-sur-Yvette, France**

[2]*Université de Lorraine, CNRS, CRM2, Nancy, France*

[3]*Institut Laue Langevin, BP156, F-38042 Grenoble France*

[4]*Vereshchagin Institute for High Pressure Physics, Russian Academy of Sciences, 142190, Troitsk, Moscow, Russia*

(Dated: July 22, 2019)

In this supplement, we provide information concerning the synthesis and macroscopic magnetic properties of the samples studied in the paper (Sec. I). Additional details concerning the treatment of the high-pressure neutron diffraction data are also given (Sec. II).

I. SAMPLES

A. Synthesis and characterization

Polycrystalline $Mn_{1-x}(Co,Rh)_xGe$ samples were synthesized under 8 GPa in a toroidal high-pressure apparatus by melting reaction with Mn, (Co,Rh) and Ge. The purity of the constituents was 99.9% (Mn, Co, Rh) and 99.999% (Ge). The pellets of well-mixed powdered constituents were placed in rock-salt pipe ampoules and then directly electrically heated to T $\approx 1600°$C. Then, the samples were quenched to room temperature before releasing the applied pressure[1]. For the current study, the samples are the same as those studied in Ref. 2. The total mass of each composition was $\approx 150 - 200$ mg.

The studied samples have been checked by X-ray diffraction in order to evaluate the amount of impurity phases within the powders (see Fig. 1). The Mn-Ge system is composed of several intermediate alloys[3], including $Mn_{11}Ge_8$, Mn_5Ge_2 and Mn_3Ge. We have thus tried to refine the powder patterns including the latter alloys, as well as CoGe and RhGe, using the `Fullprof` suite[4]. This procedure always yielded concentrations converging towards 0 (*i.e.* meaning that potential traces fall below the noise level).

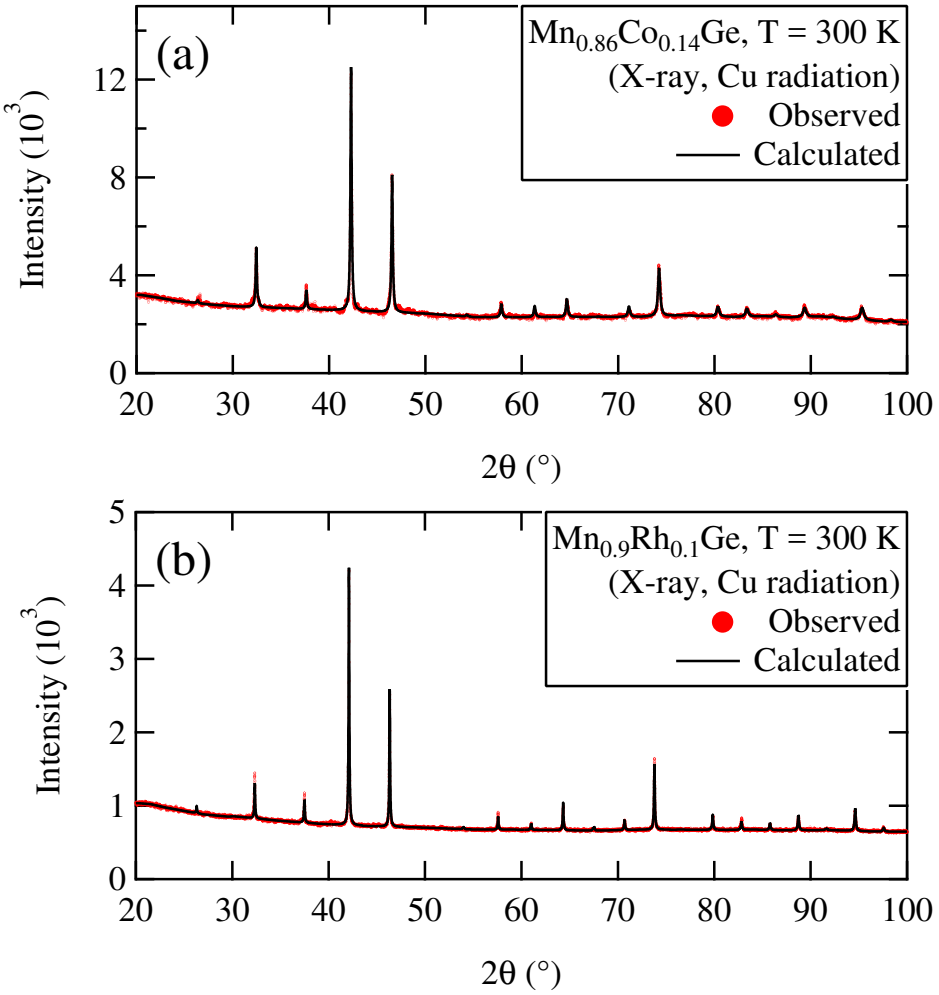

FIG. 1: X-ray powder diffractograms of the $Mn_{0.86}Co_{0.14}Ge$ **(a)** and $Mn_{0.9}Rh_{0.1}Ge$ **(b)** samples, recorded at room temperature using Cu radiation. In both panels, the measured data points (red dots) and calculated patterns (black solid line) are displayed. The part of the scattered intensity which is not captured by the refinements is entirely due to background fluctuations, which are comparatively more pronounced in the $Mn_{0.86}Co_{0.14}Ge$ case **(a)** due to a lower signal-to-noise ratio with respect to the $Mn_{0.9}Rh_{0.1}Ge$ case **(b)**.

However, it is known that the synthesis can also result in a small amount of Mn_2O_3[5] at the grain edges, as well as pure Ge[3] within the grains. Our samples indeed show the presence of these two impurity phases, with concentrations smaller than $\approx 2\%$ (see Tab. I). We note that Mn_2O_3 is an antiferromagnet (AFM) with ordering temperature close to ≈ 80 K[6]. However, its presence has no influence on the results presented in the main text, for at least two reasons:

i. The (weak) AFM contribution of Mn_2O_3 to the neutron patterns occurs at much larger angle than the helimagnetic (HM) satellites of $Mn_{1-x}(Co,Rh)_xGe$,

ii. By definition, an AFM phase does not produce stray fields and is thus magnetically decoupled from the HM (main) phase.

TABLE I: Impurity phases and their respective concentration within the samples studied in this work, as deduced from the refinement of the X-ray powder diffraction patterns of Fig. 1.

Impurity phase	Space group	In $Mn_{0.86}Co_{0.14}Ge$ (%)	In $Mn_{0.9}Rh_{0.1}Ge$ (%)
Ge	$Im\bar{3}m$ (no. 229)	0.2(0)	1.33(13)
Mn_2O_3	Pbca (no. 61)	1.99(20)	0.12(34)

B. Magnetic measurements

Temperature-dependence of static susceptibility χ in $Mn_{0.9}Rh_{0.1}Ge$ has been obtained using a Superconducting Quantum Interference Device (SQUID) magnetometer, while the $Mn_{0.86}Co_{0.14}Ge$ sample has been investigated using a Vibrating Sample Magnetometer (VSM). In both cases, we recorded data upon heating after zero-field cooling (ZFC), under an applied field H = 100 G. The temperature-dependence of χ is displayed in Fig. 2 and characteristic temperatures are given in Tab. II.

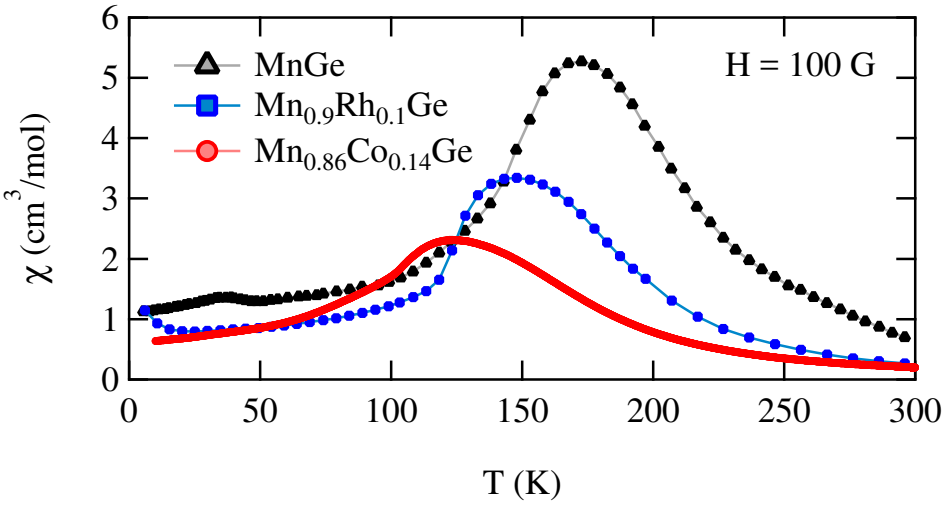

FIG. 2: Temperature dependence of the static magnetic susceptibility of $Mn_{0.86}Co_{0.14}Ge$, $Mn_{0.9}Rh_{0.1}Ge$ (this work) and MnGe (Ref. 7) obtained through a zero field cooling (ZFC) procedure, at an applied field of 100 G.

TABLE II: Curie-Weiss temperature $\theta_{\rm CW}$, obtained from a linear fit of the inverse susceptibility in the high temperature range, and position of the susceptibility peak $T_\chi^{\rm max}$ for MnGe, $Mn_{0.9}Rh_{0.1}Ge$ and $Mn_{0.86}Co_{0.14}Ge$. These values are compared with the Néel temperature $T_{\rm N}$ obtained by neutron diffraction (see main text).

Sample	$\theta_{\rm CW}$ (K)	$T_\chi^{\rm max}$ (K)	$T_{\rm N}$ (K)
MnGe	277 [Ref. 8]	172	170 [Ref. 9]
$Mn_{0.9}Rh_{0.1}Ge$	211 [Ref. 2]	147	135
$Mn_{0.86}Co_{0.14}Ge$	187 [Ref. 2]	124	123

II. NEUTRON POWDER DIFFRACTION

A. Experimental details

The neutron powder diffraction experiments presented in this manuscript have been performed on the high-intensity instrument D20 of the Institut Laue Langevin[10]. High quasi-hydrostatic pressures were applied using a so-called Paris-Edinburgh press[11], inserted within a closed-circle refrigerator allowing to reach a few Kelvin temperature. Pressure was calibrated *in situ* using the main Bragg peaks of Pb, for which the (p,V) equation of state is calibrated as a function of pressure and temperature[12]. In order to preserve quasi-hydrostatic conditions, pressure changes were systematically performed above the solidification point of the pressure transmitting medium, namely a (4:1) deuterated methanol-ethanol mixture[13].

B. Refinement of the neutron diffraction patterns

Neutron powder diffraction (NPD) patterns, corrected from a linearly interpolated background and detector efficiency, were analyzed using the `Fullprof` suite[4]. The input (*i.e.* `.pcr`) files contained three different phases:

i. A nuclear phase, corresponding to the crystallographic structure of $Mn_{1-x}(Co,Rh)_xGe$ (space group $P2_13$),

ii. A magnetic phase, with a propagation vector $\vec{Q} = (0, 0, Q_{\rm h})$,

iii. A second nuclear phase, corresponding to the crystallographic structure of Pb (space group $Fm\bar{3}m$).

In order to obtain the ordered magnetic moments displayed in Figs. 2 and 3 of main text, the nuclear and magnetic phases of the studied $Mn_{1-x}(Co,Rh)_xGe$ alloys were refined using the Rietveld method with a common scaling factor. Since nuclear scattering is proportional to tabulated cross sections, this strategy allows retrieving the values of the magnetic moments m in a self-consistent way (recalling that magnetic scattering is proportional to m^2). On the other hand, the diffraction peaks of Pb have been described using a simple profile matching (so-called Le Bail fit), which is sufficient to determine its pressure- and temperature-dependent lattice constant.

Full datasets measured at intermediate pressure values are shown in Fig. 3. The comparison with calculated patterns demonstrates the good quality of the fits. We note the systematic presence of a peak at $Q \approx 2.7\,\text{Å}^{-1}$, which is not taken into account in our refinements but most likely corresponds to the (111) reflection of Al.

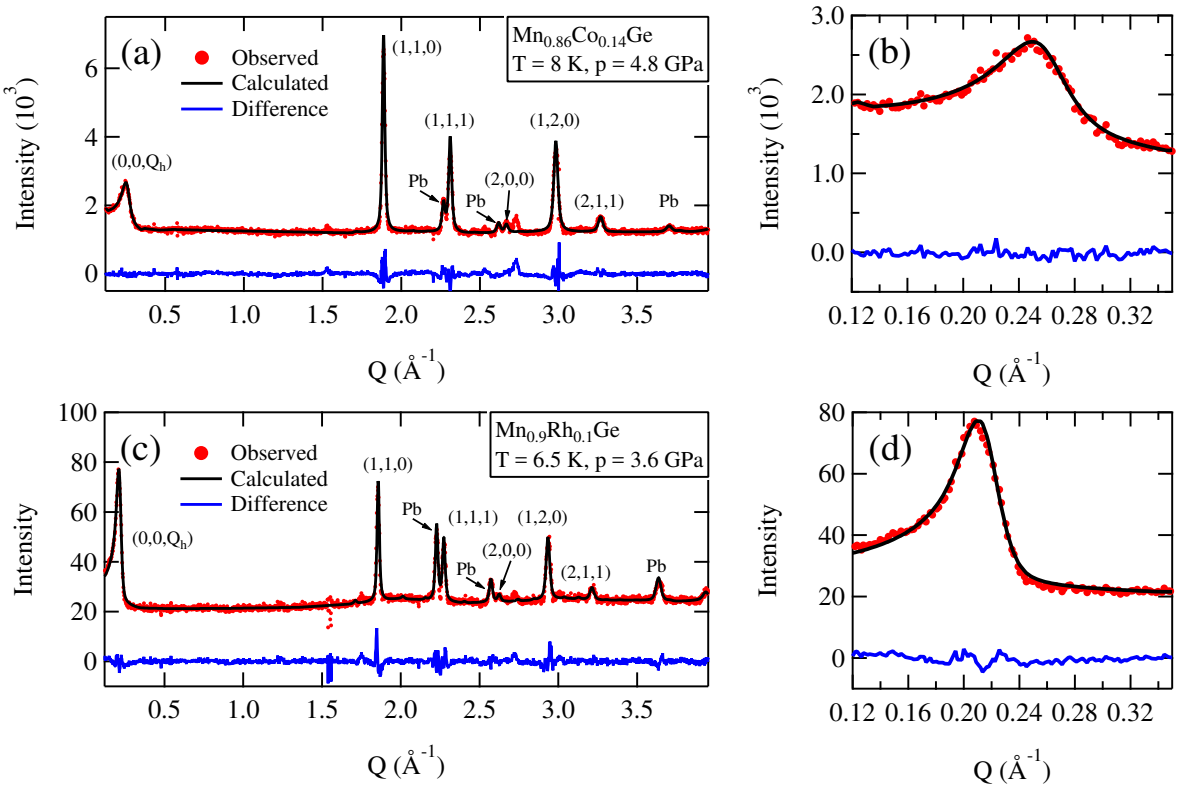

FIG. 3: **(a,c)** Low temperature NPD patterns of $Mn_{0.86}Co_{0.14}Ge$ ($p = 4.8$ GPa) and $Mn_{0.9}Rh_{0.1}Ge$ ($p = 3.6$ GPa), respectively (red dots). The calculated profiles (black line) and differences between experimental and calculated curves (blue line) are also shown. **(b,d)** Focus on the small-angle range, highlighting the $Q = 0$ helimagnetic satellite, for $Mn_{0.86}Co_{0.14}Ge$ ($p = 4.8$ GPa) and $Mn_{0.9}Rh_{0.1}Ge$ ($p = 3.6$ GPa), respectively.

C. Bragg peaks broadening and magnetic correlation lengths

In the course of the structure refinements, Bragg preaks were described by a Thompson-Cox-Hastings (TCH) pseudo-Voigt function (`Npr = 7` in `FullProf`). This peak profile is commonly used when studying helimagnetic compounds, since it includes the effects of finite horizontal beam divergence resulting in a pronounced peak asymmetry at small scattering angles (where the main magnetic satelitte is observed). This asymmetry is accounted for by assigning a value ≈ 0.1 to the parameter `D_L` in `FullProf`. The latter value is determined empirically, using datasets recorded at low pressure where the satellite intensity remains large, and fixed throughout the whole refinement process (*i.e.* at any temperatures and pressures) since it only depends on the instrumental setup.

The Gaussian part of the TCH function includes the effect of the instrumental resolution and follows a Caglioti form

$$H_{\mathrm{Gauss}} = \Delta(2\theta)_{\mathrm{Gauss}} = \left(\mathtt{U}\,\tan^2\theta + \mathtt{V}\,\tan\theta + \mathtt{W}\right)^{1/2} \quad , \tag{1}$$

where θ is half the scattering angle, while the parameters `U`, `V` and `W` are determined on a high-temperature pattern at ambient pressure, for each studied compounds.

On the other hand, the broadening of the Lorentzian part of the TCH function is either due to *(i)* pressure inhomogeneities or *(ii)* changes in magnetic correlation length. The corresponding full-width at half-maximum (FWHM) is given by

$$H_{\mathrm{Lorentz}} = \Delta(2\theta)_{\mathrm{Lorentz}} = \mathtt{X}\cdot\tan\theta + \mathtt{Y}/\cos\theta \quad , \tag{2}$$

where `X` and `Y` are pressure-dependent refined parameters (expressed in degrees in `FullProf`). From Eq. 2, it is clear that the `X` (resp. `Y`)-term will dominate at large (resp. small) scattering angle. Thus, in order to reduce the number of refined parameters, we have only refined the relevent `X` (resp. `Y`) parameter for the nuclear (resp. magnetic) phase through the whole data treatment, while `Y` (resp. `X`) was kept fixed at a zero value. Assuming a negligibly small neutron wavelength spred, one is then able to relate the angular broadening given in Eq. 2 to a momentum-transfer distribution using the kinematic expression

$$\frac{\Delta Q}{Q} = \Delta\theta\cdot\cot\theta \quad , \tag{3}$$

where θ is half the scattering angle and $\Delta\theta$ is the angular spread of the corresponding Bragg reflection (see Eqs. 1,2). Since we only consider elastic scattering, the momentum transfer Q is given by

$$Q = \frac{4\pi}{\lambda} \cdot \sin\theta \quad , \tag{4}$$

where $\lambda = 2.41$ Å is the mean neutron wavelength.

1. Pressure-induced nuclear peaks broadening

Using Eqs. 2 and 3 with $\mathtt{Y} = 0$, one gets

$$\frac{\Delta Q}{Q} = \frac{H_{\mathrm{Lorentz}}}{2} \cdot \frac{\pi}{180} \cdot \cot\theta = \frac{\pi}{360} \cdot \mathtt{X} \quad , \tag{5}$$

which gives the relative momentum transfer spread for all measured Bragg peaks. This value reflects the effects of local strains, induced by unavoidable pressure inhomogeneities. We show the pressure-dependence of $\Delta Q/Q$ for $Mn_{0.86}Co_{0.14}Ge$ and $Mn_{0.9}Rh_{0.1}Ge$ on Fig. 4. We note a slight increase upon compression. This effect remains small and is fairly comparable to what was observed for pure MnGe (Ref. 9). The raw comparison with MnGe rules out a spurious smearing of the HS-LS transition, and underscores its electronic origin, as stressed in the main text.

2. Magnetic correlation lengths

The magnetic correlation length ξ is extracted from the half-width at half-maximum (HWHM) of the $Q = 0$ magnetic satellite κ, via $\xi = 2/\kappa$. κ is obtained using Eqs. 2 and 3 with $\mathtt{X} = 0$, *i.e.*

$$\kappa = \frac{\Delta Q}{2} = \frac{1}{2}\,\Delta\theta\,\cot\theta\,Q = \frac{H_{\mathrm{Lorentz}}}{4} \cdot \frac{\pi}{180} \cdot \cot\theta \cdot Q = \frac{\pi^2}{180\,\lambda} \cdot \mathtt{Y} \quad , \tag{6}$$

yielding:

$$\xi = \frac{2}{\kappa} = \frac{360\,\lambda}{\pi^2} \,/\, \mathtt{Y} \quad . \tag{7}$$

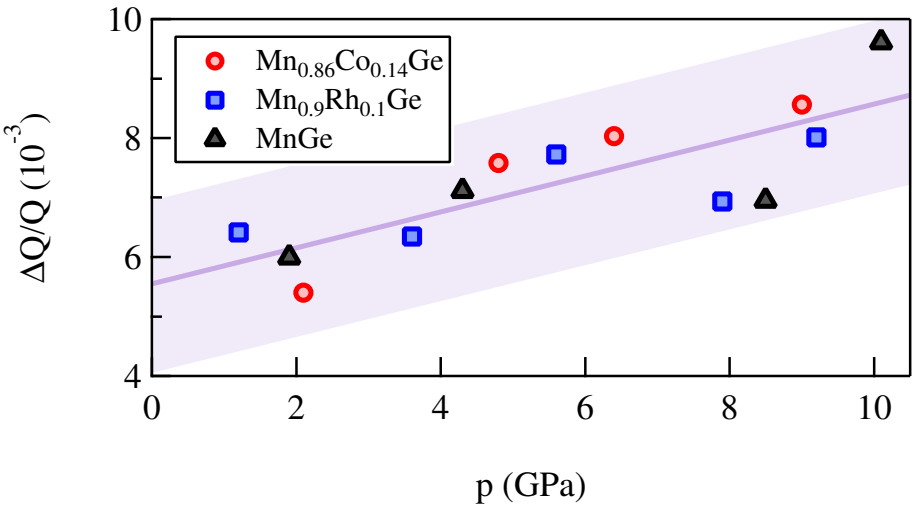

FIG. 4: Pressure-dependence of the momentum transfer spread $\Delta Q/Q$ for $Mn_{0.86}Co_{0.14}Ge$ and $Mn_{0.9}Rh_{0.1}Ge$ (this work), and MnGe (Ref. 9). Solid line is a guide to the eye.

In Fig. 5, we show the pressure-dependence of ξ for $Mn_{0.86}Co_{0.14}Ge$ and $Mn_{0.9}Rh_{0.1}Ge$, compared with the values observed for pure MnGe[9]. One immediately notes a systematic decrease of ξ upon increasing the substitution rate of Mn for Co or Rh. This effect is not surprising given that the magnetic interactions, and hence long-range ordering, must be disturbed by chemical disorder in such metallic systems. On the other hand, pressure tends to limit the correlation length but it is worth pointing out that ξ always remains much larger than the helical periodicity, suggesting that a medium to long-range order is well preserved over the whole studied pressure-range.

D. Spurious small angle peaks at high pressure in $Mn_{0.9}Rh_{0.1}Ge$

We comment on the sizeable peak, observed in the inset of Fig. 1b of main text in immediate proximity to the $Q = 0$ magnetic satellite. These patterns are obtained at the highest pressures, so that the magnetic signal becomes very weak (recalling that it is proportional to the square of the ordered moment) and even the smallest artifacts become visible. This is illustrated in Fig. 6a $Mn_{0.9}Rh_{0.1}Ge$ at an applied pressure $p = 7.9$ GPa. However, the magnetic signal can be easily isolated from its temperature dependence. On Fig. 6b, we show the result of the subtraction of a high temperature pattern (taken above the Néel temperature) from a low temperature one. This procedure results in a single magnetic Bragg peak, here located around $2\theta = 6°$. The temperature-

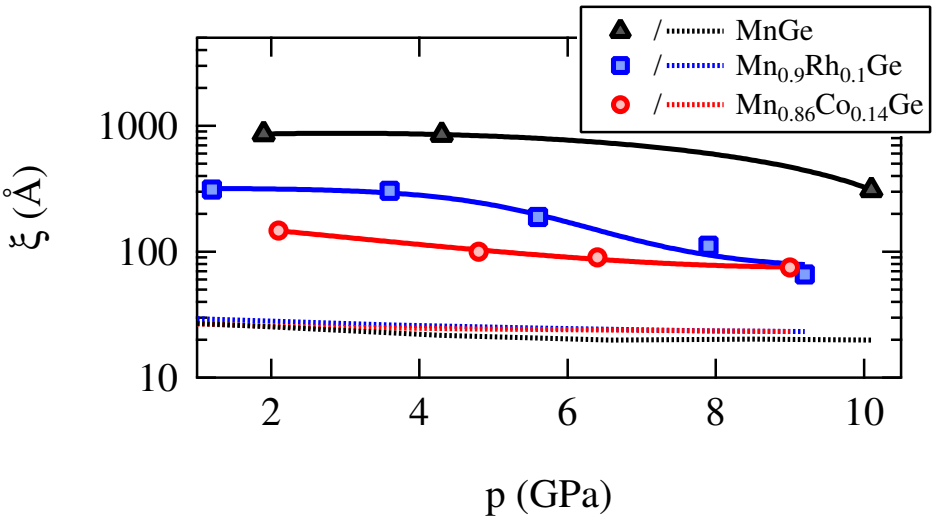

FIG. 5: **(Symbols)** Pressure-dependence of the helimagnetic correlation lengths in $Mn_{0.86}Co_{0.14}Ge$ and $Mn_{0.9}Rh_{0.1}Ge$ (this work), compared to that of pure MnGe (Ref. 9). Solid lines are guides to the eye. **(Dotted lines)** Helical periodicity λ_h for the three compounds. One sees that $\xi \gg \lambda_h$, suggesting the persitence of a medium-to-long range ordering over the whole pressure range explored in the experiments.

independent peak at $2\theta \approx 4.8°$ can therefore be considered as a locally noisy background, and as been treated as such in the course of the structural refinements presented in the main text.

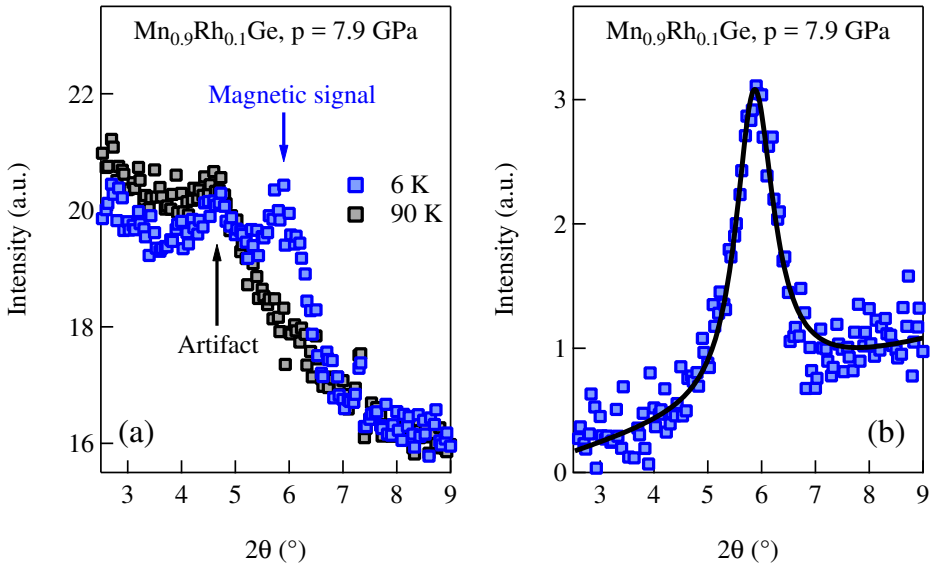

FIG. 6: **(a)** Comparison of a low (blue squares) and high (black squares) temperature patterns recorded on $Mn_{0.9}Rh_{0.1}Ge$ at an applied pressure $p = 7.9$ GPa. **(b)** The subtraction of the latter from the former results in a unique magnetic Bragg peak.

E. (p, V)-Equations of State

At relatively low compressions, the celebrated Murnaghan law is often used to model pressure-volume (p, V)-equations of state (EoS) of solids. It is given by

$$\frac{V}{V_0} = \left(1 + p\,\frac{B_0'}{B_0}\right)^{-\frac{1}{B_0'}} \quad , \tag{8}$$

where V_0 is the ambient pressure unit cell volume, B_0 the bulk modulus and B_0' its first pressure derivative.

In Fig. 7, we report the experimental low-temperature EoS of $Mn_{0.86}Co_{0.14}Ge$ and $Mn_{0.9}Rh_{0.1}Ge$ (this work), and of MnGe (Ref. 9). The doped compounds both appear to be less compressible than pure MnGe. This highlights the effect of doping on the electronic band structures of $Mn_{0.86}Co_{0.14}Ge$ and $Mn_{0.9}Rh_{0.1}Ge$, leading to locally mixed HS and LS ions. Indeed, both *ab initio* calculations[14] and x-ray diffraction[15] have shown that the LS state is always less compressible than the HS one in MnGe. For the sake of completeness, we give the parameters of the Murnaghan EoS, obtained via a fit of Eq. 8 to the NPD data.

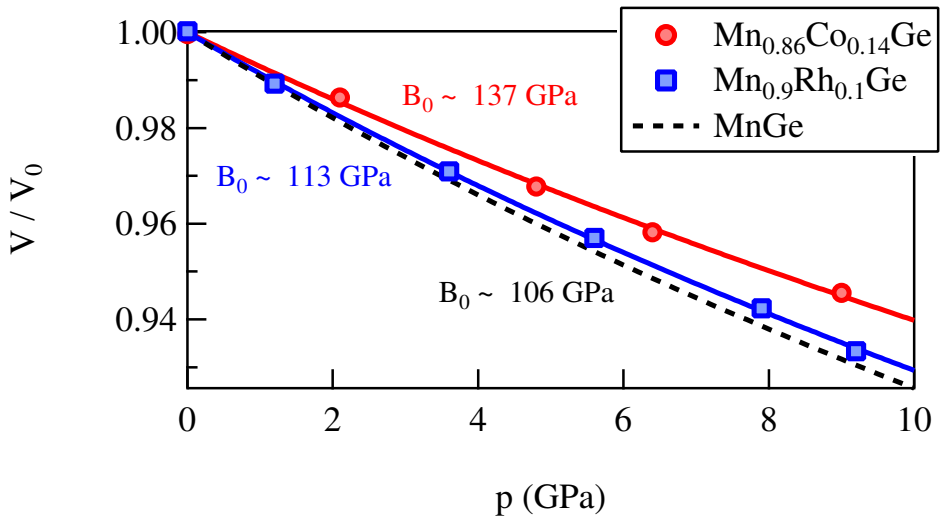

FIG. 7: (p,V) equations of state of $Mn_{0.86}Co_{0.14}Ge$ (red circles) and $Mn_{0.9}Rh_{0.1}Ge$ (blue squares). Solid lines are fit of Eq. 8 to the data, with $B_0' = 5$. Dashed line is the low-temperature EoS of pure MnGe (from Ref. 9).

TABLE III: Parameters of the Murnaghan equation (Eq. 8) describing the experimental EoS. Note that B_0' was kept fixed to a value of 5 in order to ease comparison with the reference data for pure MnGe published in Ref. 9.

Sample	V_0 (Å^3)	B_0 (GPa)	B_0'
MnGe [Ref. 9]	109.6	106	5 (fixed)
$Mn_{0.9}Rh_{0.1}Ge$ [this work]	111.3	113	5 (fixed)
$Mn_{0.86}Co_{0.14}Ge$ [this work]	108.2	137	5 (fixed)

* nicolas.martin@cea.fr

[1] A. Tsvyashchenko, V. Sidorov, L. Fomicheva, V. Krasnorussky, R. Sadykov, J. Thompson, K. Gofryk, F. Ronning, and V. Ivanov, in *Magnetism and Magnetic Materials V* (2012), vol. 190 of *Solid State Phenomena*, pp. 225–228.

[2] N. Martin, M. Deutsch, G. Chaboussant, F. Damay, P. Bonville, L. N. Fomicheva, A. V. Tsvyashchenko, U. K. Rössler, and I. Mirebeau, Phys. Rev. B **96**, 020413(R) (2017).

[3] A. Berche, J. Tedenac, and P. Jund, Intermetallics **47**, 23 (2014).

[4] J. Rodrìguez-Carvajal, Physica B **192**, 55 (1993).

[5] O. L. Makarova, A. V. Tsvyashchenko, G. André, F. Porcher, L. N. Fomicheva, N. Rey, and I. Mirebeau, Phys. Rev. B **85**, 205205 (2012).

[6] M. Regulski, R. Przenioso, I. Sosnowska, D. Hohlwein, and R. Schneider, Journal of Alloys and Compounds **362**, 236 (2004).

[7] M. Deutsch, P. Bonville, A. V. Tsvyashchenko, L. N. Fomicheva, F. Porcher, F. Damay, S. Petit, and I. Mirebeau, Phys. Rev. B **90**, 144401 (2014).

[8] R. Viennois, C. Reibel, D. Ravot, R. Debord, and S. Pailhès, Europhys. Lett. **111**, 17008 (2015).

[9] M. Deutsch, O. L. Makarova, T. C. Hansen, M. T. Fernandez-Diaz, V. A. Sidorov, A. V. Tsvyashchenko, L. N. Fomicheva, F. Porcher, S. Petit, K. Koepernik, et al., Phys. Rev. B **89**, 180407(R) (2014).

[10] T. C. Hansen, P. F. Henry, H. E. Fischer, J. Torregrossa, and P. Convert, Measurement Science and Technology **19**, 034001 (2008).

[11] S. Klotz, T. Strässle, G. Rousse, G. Hamel, and V. Pomjakushin, Applied Physics Letters **86**, 031917 (2005).

[12] S. Klotz, *Techniques in High Pressure Neutron Scattering* (CRC Press, 2012).

[13] S. Klotz, L. Paumier, G. L. March, and P. Munsch, High Pressure Research **29**, 649 (2009).

[14] U. K. Rössler, Journal of Physics: Conference Series **391**, 012104 (2012).

[15] N. Martin, M. Deutsch, J.-P. Itié, J.-P. Rueff, U. K. Rössler, K. Koepernik, L. N. Fomicheva, A. V. Tsvyashchenko, and I. Mirebeau, Phys. Rev. B **93**, 214404 (2016).